A 20-year study of melt processes over Larsen C Ice Shelf using a high-resolution regional atmospheric model: Part 2, Drivers of surface melting

E. Gilbert[1,2,] †, A. Orr[1], I. A. Renfrew[2], J. C. King[1], and T. Lachlan-Cope[1]

[1] British Antarctic Survey, High Cross, Madingley Road, Cambridge CB3 0ET, United Kingdom.

[2] School of Environmental Sciences, University of East Anglia, Norwich NR4 7TJ, United Kingdom.

Corresponding author: Ella Gilbert (ella.gilbert@reading.ac.uk)

† Present address: Department of Meteorology, University of Reading, Whiteknights Road, Reading RG6 6ET, United Kingdom.

Key words: Larsen C ice shelf; Antarctic Peninsula; regional climate modelling; surface melt; meteorology; model hindcast

Key points:

- The amount of surface melting on Larsen C is driven mostly by sunny conditions, followed by foehn events, cloud and large-scale circulation
- Deep Amundsen Sea Low, positive Southern Annular Mode, and El Niño conditions enhance surface melting
- Drivers of surface melting overlap and interact

Abstract

Quantifying the relative importance of the atmospheric drivers of surface melting on the Larsen C ice shelf is critical in the context of recent and future climate change. Here, we present analysis of a new multi-decadal, high-resolution model hindcast using the Met Office Unified Model (MetUM), described in part 1 of this study. We evaluate the contribution of various atmospheric conditions in order to identify the most significant causes of melting over the recent past. We find the primary driver of surface melting on Larsen C is solar radiation. Foehn events are the second most important contributor to surface melting, especially in non-summer seasons when relatively less solar radiation is received at the surface of the ice shelf. Thirdly, cloud influences surface melting via its impact on the surface energy balance (SEB); when the surface temperature is warm enough, cloud can initiate or prolong periods of melting. Lastly, large-scale circulation patterns such as the Southern Annular Mode (SAM), El Niño Southern Oscillation (ENSO) and Amundsen Sea Low (ASL) control surface melting on Larsen C by influencing the local meteorological conditions and SEB. These drivers of melting interact and overlap, for example, the SAM influences the frequency of foehn, which are commonly associated with leeside cloud clearances and sunnier conditions. Ultimately, these drivers matter because sustained surface melting on Larsen C could destabilise the ice shelf via hydrofracturing, which would have consequences for the fate of the ice shelf and sea levels worldwide.

Plain Language Summary

In order to predict the future of the largest remaining ice shelf on the Antarctic Peninsula - Larsen C – we must understand what is causing it to melt at the surface. We use results from a new model dataset to explore which causes of melting are the most important. Our results show that the most dominant factor is solar radiation, especially in summer, while hot, dry foehn winds are the second most important cause of melting. Foehn winds are an especially significant cause of melting in non-summer seasons. The third driver of surface melting is cloud, because clouds can affect how much energy is received at the surface of the ice shelf. When it is warm enough, clouds can initiate or sustain melting. The final cause of melting is large-scale atmospheric circulation patterns, which can establish the conditions that promote melting, such as sunny, cloudy or foehn periods. These melt drivers interact with one another and can add to or take away from the effects of other causes of melting. These melt drivers matter because ongoing melt can cause an ice shelf to collapse, and therefore indirectly contribute to sea level rise.

1 Introduction

Atmospheric drivers of surface melting were implicated in the collapse of the Larsen A and B ice shelves that previously neighboured Larsen C - the largest remaining ice shelf on the eastern side of the Antarctic Peninsula - by increasing firn densification, meltwater ponding and ultimately hydrofracturing and disintegration (Scambos et al., 2000; 2003; Bell et al., 2018). In particular, the large-scale circumpolar westerly circulation is known to have an important role in the Antarctic Peninsula region by influencing local atmospheric conditions via its effect on foehn winds. Foehn winds cause leeside warming and associated melting over these ice shelves (van Lipzig et al., 2008; Orr et al., 2008; 2021; Cape et al., 2015; Elvidge et al. 2015, 2016; King et al. 2017; Kuipers Munneke et al., 2018), and a distinct west-east gradient in melting over Larsen C (Bevan et al., 2018; Elvidge et al. 2020; Gilbert et al., 2021). Large-scale circulation variability in the Southern Hemisphere is strongly influenced by the Southern Annular Mode (SAM). The SAM underwent a positive trend from the 1960s to mid-1990s, particularly in austral summer (December, January, February; DJF), causing flow to be more dominantly westerly (Marshall, 2003; Marshall et al., 2006; Fogt & Marshall, 2020), although there has not been a significant trend since then. Stronger westerly flow associated with a more positive SAM strengthened the flow impinging on the Antarctic Peninsula, resulting in increased foehn-induced warming over the ice shelves (Orr et al., 2008; Cape et al., 2015; Datta et al., 2019).

The SAM is strongly correlated with the strength of the Amundsen Sea Low (ASL), which is a climatological low-pressure centre in the Amundsen/Bellingshausen Seas to the west of the Antarctic Peninsula, that influences near-surface wind, temperature and sea ice concentration, and thus primarily temperatures on the western side of the Antarctic Peninsula (King, 1994; Turner et al., 2013; Hosking et al., 2013). The El Niño Southern Oscillation

(ENSO) teleconnection also influences the ASL, primarily during austral winter (June, July, August; JJA) and spring (September, October, November; SON) (Clem et al., 2016). The SAM and ENSO are shown to be anti-correlated throughout the instrumental record (Fogt et al., 2011; Dätwyler et al., 2020), and by influencing the strength of the ASL can affect the advection of warm maritime air across the Antarctic Peninsula and thus atmospheric conditions (including foehn events) over its eastern side.

As the high mountains (~2000 m) running along the spine of the Antarctic Peninsula present a significant barrier to prevailing westerly winds, they therefore separate the relatively warm, maritime environment to the west from a much cooler continental climate on the eastern side (Orr et al., 2004). Cold air masses on the eastern side of the Antarctic Peninsula can also be blocked by the high orography, resulting in the formation of strong southerly or 'barrier' winds flowing along the eastern side of the Peninsula (Schwerdtfeger, et al. 1975; Parish, 1983), which can therefore affect temperatures over Larsen C.

Some attempts have been made to link specific atmospheric drivers to increased melting over the ice shelves on the eastern side of the Antarctic Peninsula. For instance, Cape et al. (2015) use satellite and Automatic Weather Station (AWS) data to correlate monthly Antarctic Peninsula foehn occurrence with backscatter-derived surface melt and find the strongest relationships on the Larsen A and B ice shelves and in inlets in the northwest of Larsen C ice shelf. Kuipers Munneke et al. (2018) demonstrate that a foehn event drove enhanced surface melting across Larsen C during austral autumn (March, April, May; MAM) 2016. Elvidge et al. (2020) also find that foehn winds are the dominant meteorological driver of melt across Larsen C, with the primary cause of melting attributed to incoming shortwave (SW) radiation, a result also reported by Gilbert et al. (2020) for DJF 2011. Recall foehn events are commonly associated with leeside cloud clearance and thus enhanced SW radiation (e.g., Takane and Kusaka 2011).

Gilbert et al. (2020) identify cloud phase as a crucial determinant of melting over Larsen C because optically thick clouds with larger ice or liquid water paths (IWP or LWP) decrease downward SW radiation and increase downward longwave (LW) radiation, and whether the cloud enhances or suppresses melt depends on the balance between these radiative effects (Hofer et al., 2019). Optically thick cloud is shown by Ghiz et al. (2021) to increase downward LW fluxes enough to initiate and prolong periods of melting in West Antarctica, while optically thin liquid-bearing cloud can also enhance melting by increasing the total downward radiative flux, a phenomenon also noted in Greenland by Bennartz et al. (2013). Although demonstrated for short periods (Gilbert et al., 2020), the importance of cloud-mediated melting on Larsen C has not been examined over multiple decades.

Regional climate models (RCMs) are commonly used to assess the role of atmospheric drivers of melt on Larsen C due to the dearth of long-term observations (e.g. Orr et al., 2008, 2021; Elvidge et al., 2015; 2016; 2020; Turton et al., 2018;

2020; Kuipers Munneke et al., 2018; Wiesenekker et al., 2018; Datta et al., 2019; Laffin et al., 2021; Gilbert et al., 2021). However, many of these studies have focused on particular meteorological phenomena, especially the role of foehn winds (e.g. Turton et al., 2018; 2020; Datta et al., 2019; Laffin et al., 2021; Orr et al., 2021), and/or have examined melt over a relatively short timeframe (e.g. Kuipers Munneke et al., 2018; Gilbert et al., 2020; Elvidge et al., 2020). To date, no work has attempted to assess the relative importance of the first-order drivers of surface melting on Larsen C (i.e., SW radiation, foehn, cloud cover and phase, and large-scale circulation patterns like the SAM, ENSO and ASL) on the surface energy balance (SEB) or melting over a multi-decadal time period.

Although van Wessem et al. (2015) produced a near-surface climatology of the Antarctic Peninsula using RACMO2.3 (Regional Atmospheric Climate Model) at a spatial resolution of 5.5 km, this poorly simulated foehn winds due to it being a hydrostatic model and having insufficient resolution to resolve the complex dynamics (Orr et al., 2021). Further, only temperature and wind speed were archived, limiting the potential for analysis. Wiesenekker et al. (2018) diagnose foehn wind occurrence between 1979-2016 at Cabinet Inlet on Larsen C, situated close to the foot of the eastern slopes of the Antarctic Peninsula, from AWS and RACMO2.3 model data, but do not relate this to the SEB. King et al. (2015) comprehensively evaluate the ability of three RCMs to reproduce observed meteorology and SEB on Larsen C during summer 2010/11, but the period is short – just one month. Gilbert et al. (2020) evaluate melting on Larsen C over this same one-month period but focus solely on the role of cloud on melt. Similarly, Elvidge et al. (2020) use the regional configuration of the UK Met Office Unified Model (MetUM) at 1.5 km resolution to assess the role of various SEB regimes in driving melt on Larsen C and include a thorough investigation of the role of solar radiation and foehn and the conditions that produce these, but this process-focused study is limited in its duration to six months. Datta et al. (2019) use the MAR (Modèle Atmosphérique Régionale) model at 7.5 km resolution to evaluate the effect of foehn events on the evolution of the snowpack during the period 1982-2017 and find three regimes in which surface melting occurs, related to foehn winds and cloud occurrence. However, the focus of their study is on the evolution of firn and the snowpack, rather than quantifying the atmospheric processes that influence the SEB regime and surface melting. Laffin et al. (2021) examine the impact of foehn winds on melting during 1979–2018 using machine learning and the RACMO2.3 model, and Turton et al. (2020) combine observations and model output from AMPS (Antarctic Mesoscale Prediction System) to explore seasonal patterns in foehn-driven surface melt. Lastly, Bozkurt et al. (2020) use the WRF (Weather Research and Forecasting) model at 15 km resolution to produce a hindcast for the Antarctic Peninsula over the period 1991-2015, which again is insufficiently fine-scale to adequately resolve important features such as foehn winds.

Given these shortfalls, the aim of this investigation is to robustly quantify the importance of the various drivers of Larsen C surface melting over a multi-

decadal period, which is critical for understanding its stability in the context of past, present and future change. For example, both Trusel et al. (2015) and Gilbert & Kittel (2021) identify Larsen C as being vulnerable to hydrofracturing-mediated collapse as the climate warms. By bringing together the many atmospheric drivers or conditions that are demonstrably important in the region, such as foehn, cloud phase and large-scale circulation variability, this study will comprehensively determine their impact on the SEB and surface melting over Larsen C.

It will do this by comprehensively examining output from the high-resolution multi-decadal MetUM hindcast of the Antarctic Peninsula described in Part 1 of this study (Gilbert et al., 2021), which included a validation of the model SEB against AWS measurements on Larsen C. Part 1 showed that the hindcast is capable of representing the foehn-induced east-west gradient in surface melting on Larsen C observed by satellites (Bevan et al., 2018), i.e., indicating that it is able to reasonably represent foehn-associated flow. It further shows that the model captures the observed frequency of foehn events over Larsen C, and adequately simulates near-surface meteorology. The MetUM is therefore a useful tool for studying the dominant conditions that influence surface melting on the Larsen C ice shelf.

2 Data & Methods

2.1 The surface energy balance and surface melt

The influence of atmospheric processes on surface melting is quantified by examining their effect on the SEB, defined as the balance between upwelling and downwelling components of SW and LW radiation, $SW_{\uparrow}$, $SW_{\downarrow}$, $LW_{\uparrow}$ and $LW_{\downarrow}$ respectively, and the latent, sensible and ground heat fluxes, H_S, H_L and G_S, respectively, and which is formulated as:

$$E_{\text{tot}} = \text{LW}_{\uparrow} + \text{LW}_{\downarrow} + \text{SW}_{\uparrow} + \text{SW}_{\downarrow} + H_S + H_L + G_S \quad (1)$$

where fluxes directed towards the snow surface are defined as positive. Surface melt energy, E_{melt}, is positive when the sum of fluxes, E_{tot}, is positive and surface temperature T_S is at or above the melting point, i.e.:

$$E_{\text{melt}} = \begin{cases} E_{\text{tot}} & T_S \geq 0℃ \\ 0 & T_S < 0℃ \end{cases} \quad (2)$$

2.2 The MetUM model

As the MetUM hindcast is comprehensively described and evaluated in Gilbert et al. (2021), this section will only give brief details of the simulation. The hindcast uses a spatial resolution of 4 km over a domain that covers the central Antarctic Peninsula, centred on the Larsen C ice shelf (Figure 1). Boundary conditions are from ERA-Interim. It has output at three and six hourly temporal resolution for one/two-dimensional and three-dimensional variables, respectively. The variables archived include SEB terms (turbulent and radiative fluxes), near-surface meteorology (winds, humidity, temperatures, pressure etc.), cloud fields

(water paths, mass mixing ratios, cloud fractions etc.) and surface melt terms as well as three dimensional winds, potential temperature, air temperature and specific humidity on model and pressure levels. A full description of the outputs can be found at Gilbert (2020a).

On average, Gilbert et al. (2021) found that the MetUM hindcast simulates conditions over Larsen C that are slightly warmer, windier and moister compared to observations from AWSs, and that net radiation, $R_{net,}$ (LW_{net} + SW_{net}) and E_{melt} are under-estimated. The hindcast represents many components of the SEB well, for example model SW albedo is simulated to within 1% and 3% of observed values at inlet and ice shelf AWSs, respectively (with inlet stations situated along the western edge of the ice shelf at the base of the Antarctic Peninsula, and ice shelf stations situated over the homogeneous ice to the east of the Peninsula). Downwelling radiative fluxes are simulated within 10% of observed values at both inlet and ice shelf stations. However, positive T_S and consequently $LW_{\uparrow}$ biases result in negative R_{net} and E_{melt} biases that are more pronounced at inlet stations, and during DJF. More detailed validation can be found in Part 1.

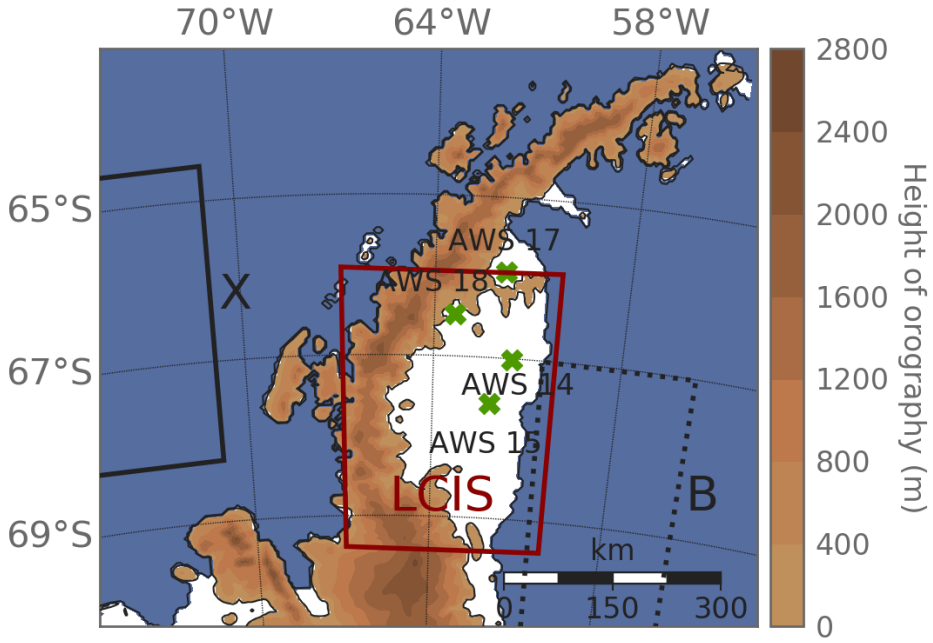

Figure 1. Map of the Antarctic Peninsula MetUM hindcast model domain, with the locations of the four AWSs used for validation indicated with green crosses. The map is centred on the Larsen C ice shelf and its tributary inlets, and also shows the remnant Larsen B ice shelf on which AWS 17 is located. The mean modelled height of orography is indicated with coloured contours and is derived

from the RAMP 200 m elevation model (Liu, 2015). The three regions used in the diagnosis of conditions influencing melt are also shown. Abbreviations used in the plot are as follows. "X": region in which u_{Z1} is calculated, used for diagnosing foehn conditions, "B": region for diagnosing barrier wind conditions, "LCIS": Larsen C box used to calculate means for high and low melt, high and low LWP, sunny, cloudy and clear conditions.

2.3 Diagnosing dominant conditions

The relative importance of various drivers of surface melting is assessed by examining periods when certain conditions prevail, which have been identified from the literature summarised in section 1. These include: sunny, foehn, cloudy, clear, high/low LWP, barrier wind, ASL, positive/negative SAM, positive/negative ENSO, and high/low melt conditions. These are listed in Table 1 and defined in full below. Large-scale circulation patterns (i.e., SAM, ASL and ENSO) are diagnosed using observed indices. All other conditions are determined from model output and diagnosed from "indicator variables", which are the parameters that reveal whether or not certain conditions prevail. The regions used for averaging indicator variables are shown in Figure 1 and data sources and treatments are described in detail in the supplementary information (Table S1).

Foehn conditions are diagnosed when foehn winds are detected in the model data for at least six 3-hour periods in a day at the locations of all of the three AWSs on the Larsen C ice shelf (AWS 14, 15 and 18; See Figure 1 for their location), which may indicate either foehn conditions occurring persistently at one AWS (i.e. for 18+ hours in a day) or foehn occurring at all three AWSs (i.e. for 6+ hours in a day), or a combination of these situations. Foehn events at each AWS location are detected using the isentrope-based method described in Gilbert et al. (2021), which diagnoses foehn conditions over Larsen C if the following occur: a) the mean upstream zonal flow impinging on the Antarctic Peninsula between approximately 250-2500m altitude, u_{Z1}, has a clear westerly component (i.e., u_{Z1} $2\ m\ s^{-1}$) so that the oncoming flow can be forced over the Peninsula, b) the upwind isentrope at altitude Z1 (~2500 m) falls downstream of the Peninsula (over Larsen C) by an altitude of at least 500 m over a 6-hour period, and c) warming of the atmospheric column is simulated over Larsen C, resulting in warming and drying at the ice shelf surface.

Sunny conditions are diagnosed when the mean incoming solar radiative flux ($SW_{\downarrow}$) over the Larsen C ice shelf (averaged over the region marked "LCIS" in Figure 1) exceeds the 75^{th} percentile of 20-year mean $SW_{\downarrow}$ for the day of the year considered. $SW_{\downarrow}$ is therefore the "indicator variable" that enables the detection of these conditions. Cloudy and clear conditions are detected using cloud fraction, averaged over the "LCIS" region in Figure 1, according to the thresholds of Kay et al. (2008). "Cloudy" conditions are diagnosed when the mean cloud fraction exceeds 0.75, while "clear" conditions occur when cloud fraction is below 0.31. High and low LWP conditions occur when the mean LWP

over the "LCIS" region falls above and below the 75th and 25th percentiles for that day of the year, respectively, in a manner similar to the diagnosis of sunny conditions. High and low IWP conditions are not examined because liquid cloud was shown to exert a more important control on the SEB and surface melting over Larsen C in Gilbert et al. (2020).

Barrier wind conditions are diagnosed when mean 10 m meridional wind speeds in the Weddell Sea region (marked "B" in Figure 1) exceed 5 m s^{-1}, indicative of strong near-surface southerly flow. Modelled 20-year mean meridional wind speeds in this region are 1.13 m s^{-1}, so this threshold represents a significant increase. High and low melt periods are determined using the 75th and 25th percentiles of meltwater production, respectively, averaged over the "LCIS" region.

The daily mean SAM index is that of the US National Oceanic and Atmospheric Administration (NOAA)'s National Weather Service Climate Prediction Centre and is calculated from National Center for Environmental Prediction/National Center for Atmospheric Research reanalysis at 2.5° × 2.5° resolution (CCP, 2005). Positive and negative SAM periods ae abbreviated as "SAM+" and "SAM-", respectively. The Nino3.4 dataset (Reynolds et al., 2007), which is used by the World Meteorological Organisation and NOAA to diagnose El Niño and La Niña events, is used to diagnose the phase of ENSO at daily frequency. El Niño and La Niña periods are abbreviated to "ENSO-" and "ENSO+", respectively. Positive and negative phases of these circulation modes are detected when the index is above/below plus/minus one standard deviation of the time series 1998-2017. Positive and negative ENSO periods are diagnosed when three-month running mean anomalies are above or below 0.5°C or -0.5°C, respectively, according to the method of NOAA (see https://www.weather.gov/fwd/indices, accessed 30/06/2020).

The influence of the ASL is examined using the observed index of Hosking et al. (2013), which measures the depth and longitude of the ASL. Deep ASL conditions (hereafter referred to simply as 'ASL conditions') are diagnosed when the relative central pressure is less than the 25th percentile and its latitude is north of 70°S, where it will have a more notable impact on conditions over Larsen C. (Here the relative central pressure is defined by subtracting the actual central pressure from an area-averaged pressure over the ASL sector, defined as 170°—298° E, 80°—60° S, see Hosking et al., 2013).

2.4 Analysis methods

The study employs two primary analysis methods. Firstly, Pearson correlation coefficients (r values) between pertinent variables (such as E_{melt} and $SW_{\downarrow}$) are examined to quantify the strength of the relationships between modelled variables. The statistical significance of the relationship is also calculated as a two-sided p value. Secondly, a composite approach is used, in a similar manner to Deb et al. (2018). During periods when particular conditions are diagnosed as described above, mean meteorological variables (3-hourly mean 10 m winds,

1.5 m air temperature and MSLP) and SEB parameters (SW, LW, H_S, H_L, E_{tot} and E_{melt}) are averaged to produce a composite that represents the meteorological state during these conditions. The relative proportion of total melt produced during conditions characteristic of each melt driver, as well as the proportion of time in which those conditions occur were also calculated in order to quantify the importance of each driver of surface melt on Larsen C. All analysis was performed seasonally and is based on model output for the 1998-2017 period.

3 Results & Discussion

The drivers of surface melting are first considered by examining the "high melt" composites. After this, we assess the role of the most important controls on surface melt.

3.1 "High melt" composites

Figure 2 shows composited mean seasonal conditions during high melt conditions (melt amount $> 75^{th}$ percentile, Table 1); panels a-d show daily near-surface meteorological conditions, while daily E_{melt} anomalies relative to the climatology for 1998-2017 are shown in panels e-h. Figure 2 shows that for all seasons, instances of high melting over Larsen C occur during periods of north-westerly flow, which produces cross-peninsula winds and therefore is conducive to establishing foehn conditions, and/or the advection of relatively warm and moist maritime air across the Antarctic Peninsula.

Consistent with Kuipers Munneke et al. (2018) and Elvidge et al. (2020), these conditions are associated with significant increases in H_S, and consequently in E_{tot} and E_{melt} over Larsen C, driving surface melting particularly during DJF when surface temperature is higher. During DJF high melt conditions are associated with high $SW_{\downarrow}$ fluxes, causing temperatures to be at the melt point more frequently. Compared to the other seasons, it is also associated with comparatively weaker cross-peninsula flow and comparatively small T_{max} anomalies (Figure 2b). Around 63% of DJF meltwater production over Larsen C occurs in high melt periods (Table 1), which take place over the entire ice shelf (Figure 2e). This differs from SON, MAM and JJA, when melting occurs almost exclusively during intense melt events (Kuipers Munneke et al., 2018) associated with cross-peninsula flow and is confined to the western regions of the ice shelf (Figure 2f,g,h), with 93%, 98% and 97% of seasonal meltwater production occurring in just 9%, 7% and <1% of the time, respectively (Table 1).

The following sub-sections examine in turn the role of each of the various conditions described in Section 2.3 on surface melt over Larsen C.

Table 1. Percentage of total modelled meltwater production (%) associated with the conditions evaluated during each season for the hindcast period, and the frequency at which they occur (%). Prevailing conditions are abbreviated as defined in the main text, and as follows. "Low melt": mean meltwater production $< 25^{th}$ percentile; "High melt": mean meltwater production $> 75^{th}$ percentile;

"Sunny": SW↓ > 75th percentile; "Foehn": foehn conditions; "Cloudy": mean cloud fraction > 0.75; "Clear": mean cloud fraction < 0.31; "Low LWP": mean LWP < 25th percentile; "High LWP": mean LWP > 75th percentile "SAM+": positive SAM; "SAM-": negative SAM; "ENSO+" positive ENSO (La Niña conditions); "ENSO-": negative ENSO (El Niño conditions); "ASL": deep Amundsen Sea Low; "Barrier": low-level southerly barrier jet over the Weddell Sea region. Note that high and low melt conditions are responses to forcing (such as foehn conditions or SW radiation) rather than causes of melting themselves and are used to guide the analysis in section 3.

	DJF	**MAM**	**JJA**	**SON**		
	Melt amount	**Frequency**	**Melt amount**	**Frequency**	**Melt amount**	**Frequency**
Low melt	0.8	24.5	0.0	7.1	0.1	0.6
High melt	63.0	24.5	97.6	7.2	96.7	0.7
Sunny	41.7	25.0	47.1	25.0	0.3	25.0
Foehn	22.4	18.7	54.8	16.7	97.3	20.9
Cloudy	50.2	61.6	69.1	54.6	95.5	56.9
Clear	9.8	7.8	2.4	9.2	0.0	10.8
Low LWP	32.0	25.0	4.2	25.0	0.0	25.0
High LWP	15.2	25.0	44.4	25.0	90.7	25.0
SAM+	25.0	21.9	38.9	17.3	21.9	22.2
SAM-	8.5	9.3	0.5	10.7	0.1	15.6
ENSO+	38.1	40.0	17.1	35.5	1.5	15.3
ENSO-	34.6	33.5	65.6	23.2	3.8	15.2
ASL	6.4	3.3	19.9	11.7	0.2	11.6
Barrier	3.8	10.8	0.0	15.9	0.0	19.2

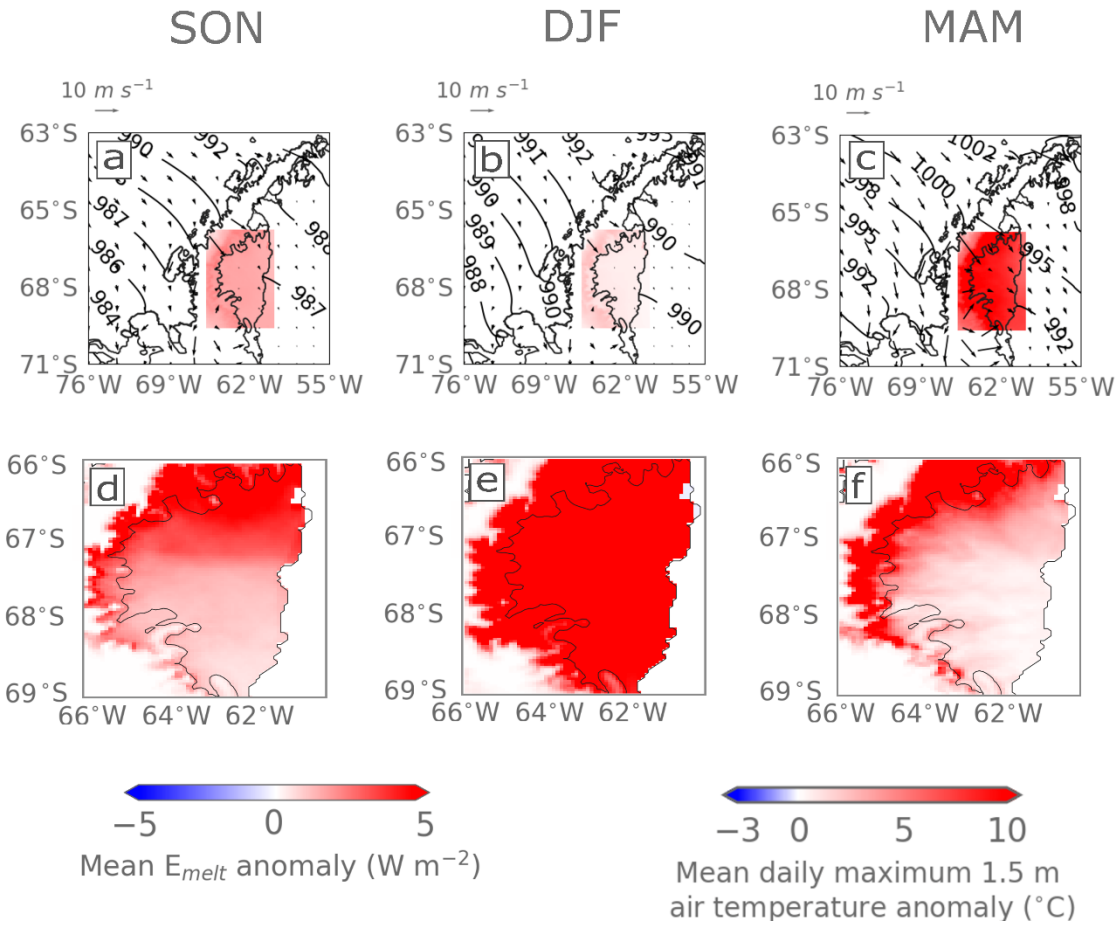

Figure 2. Composited daily mean conditions during "high melt" conditions (melt amount $> 75^{\text{th}}$ percentile) for spring (SON), summer (DJF), and autumn (MAM), for the hindcast period. JJA is not shown because the amount of melting occurring during winter is negligible. Panels a) to c) show mean synoptic meteorological conditions, where coloured shading shows the daily maximum 1.5 m air temperature anomaly (T_{max}; units °C), and contours and vectors give mean sea level pressure (hPa) and 10 m wind speed and direction, respectively. Panels d) to f) show anomalies in surface melt (E_{melt}; units W m^{-2}). Anomalies are computed relative to the 1998-2017 model climatology. Synoptic meteorology plots show the wider Antarctic Peninsula region, while the E_{melt} plots focus on the Larsen C ice shelf.

3.2 Drivers of modelled surface meltwater production

3.2.1 Solar radiation

Table 2 shows Pearson correlation coefficients between daily E_{melt} and other SEB components over the Larsen C ice shelf for the entire hindcast period.

The largest annual correlation between E_{melt} and the fluxes in Table 2 is with SW_{net} ($r_{SWnet,melt} = 0.56$). This relationship is also seen in DJF ($r_{SWnet,melt} = 0.45$), which supports the findings of Gilbert et al. (2020) that SW radiation is a dominant driver of summertime surface melting. 90% of hindcast-simulated surface melting occurs in DJF (not shown) when $SW_{\downarrow}$ is highest, which suggests that meltwater production is driven predominantly by $SW_{\downarrow}$. This result is consistent with Elvidge et al. (2020) and Gilbert (2020b), who also find that SW radiation is the dominant cause of surface melting during summer. Correlations are insignificant in JJA (Table 2) when there is very little $SW_{\downarrow}$ and <0.1 % of meltwater production occurs. For this reason, JJA is not included in Figure 2 or subsequent composite figures.

Table 2. Pearson correlation coefficients (r) between E_{melt} and $SW_{\downarrow}$, SW_{net}, $LW_{\downarrow}$, LW_{net}, H_S, and H_L over the Larsen C ice shelf during each season, and annually, for the hindcast period. Only values that are significant at the 99% level are shown.

	DJF	**MAM**	**JJA**	**SON**	**ANN**
$\mathbf{SW_{\downarrow}}$	0.42	-	-	0.29	0.52
$\mathbf{SW_{net}}$	0.45	-	-	0.33	0.56
$\mathbf{LW_{\downarrow}}$	-	0.15	-	0.22	0.33
$\mathbf{LW_{net}}$	-0.19	-	-	-	-0.12
$\mathbf{H_S}$	0.38	0.28	0.11	-	-
$\mathbf{H_L}$	0.15	0.08	-	-0.14	-0.19

Table 1 shows that 'sunny' conditions ($SW_{\downarrow} > 75^{th}$ percentile) occur 25% of the time in DJF, yet account for 42% of total DJF meltwater production (and around 38% of the annual total, not shown in Table 1). The proportion of meltwater production associated with 'sunny' conditions increases to 47% and 75% in MAM and SON, respectively (Table 1), indicating that periods of above-average insolation are important for driving surface melt during these seasons, particularly during SON. Once the frequency of occurrence is accounted for, 'sunny' conditions account for the highest percentage of meltwater production of any driver in DJF and SON. This is also apparent from Figure 3, which shows that the largest DJF E_{melt} anomalies are associated with 'sunny' conditions. 'Sunny' conditions are associated with extensive positive E_{melt} anomalies across the ice shelf, especially during DJF (Figure 3e) but also during SON (Figure 3d), partly because extensive T_{max} anomalies occur during such periods, especially in DJF and MAM (Figure 3b,c).

The co-occurrence of 'high melt' and 'sunny' conditions can also be used to demonstrate the importance of SW radiation in driving more intense melt events. During SON, DJF and MAM, 'high melt' and 'sunny' conditions co-occur 73%, 50% and 46% of the time, respectively (not shown). The high co-occurrence during SON suggests that SW radiation is especially important for driving the

most intense melt events, whereas periods in DJF when $SW_{\downarrow}$ is more similar to climatological conditions can still account for a comparatively large amount of melting. Because 96% of total annual melt occurs during these two seasons, these results suggest that SW radiation is the most important driver of surface melting on Larsen C overall.

3.2.2 Foehn

The frequency of foehn events at inlet and ice shelf stations is diagnosed using the isentrope-based method described in section 2.3 and composites of near-surface meteorology and surface fluxes when foehn winds are detected are shown in panels g-l of Figure 3. Foehn conditions are associated with strong north-westerly flow and positive T_{max} anomalies in all seasons (Figures 3g-i), which has different effects on E_{melt} in different seasons (Figures 3j-l). During JJA (not shown), temperatures are largely too low for melting to occur, while in DJF, foehn events are associated with positive E_{melt} anomalies that are distributed fairly evenly across Larsen C (Figure 3k), with slightly higher anomalies in inlets below the peak of orography, i.e., a zonal gradient in melt. E_{melt} anomalies in SON (Figure 3j) are similarly extensive, but of lower magnitude, whereas much more intense, confined melting is simulated in the immediate lee of steep topography in MAM (Figure 3l).

Using the isentrope-based method, foehn conditions are diagnosed 92%, 49%, 40% and 24% of the time that 'high melt' conditions shown in Figure 2 also occur in JJA, MAM, SON and DJF, respectively (not shown). Foehn are less important for driving intense melt events in DJF because foehn occur less frequently (19% of the time, Table 1) and have less impact (accounting for 22% of melt, Table 1) because SW radiation is the primary driver of melting in summer and temperatures are already closer to the melting point. This is evident in Figure 3 from the lower T_{max} anomalies associated with foehn conditions (panels j-l). As shown in section 3.2.1, SW radiation is the most important driver of intense melt events in SON (Figure 3d), although the foehn conditions are still associated with 48% of SON melt despite occurring only 24% of the time (Table 1). During MAM, foehn is far more important than SW, with 'foehn' conditions associated with 55% of MAM melting, despite occurring just 17% of the time (Table 1). This is also apparent from Figures 3 (panels f and l) and 4.

The above results show that foehn events are an important driver of surface melting over the Larsen C ice shelf year-round but are especially important in non-summer seasons. As discussed earlier, foehn events are associated with positive H_S fluxes because they bring warm air to the surface. Accordingly, positive correlations are simulated between E_{melt} and H_S in DJF, JJA and MAM (Table 2), although these are larger during DJF and MAM. This result is consistent with Elvidge et al. (2020), who find that regimes dominated by large positive H_S fluxes account for a large amount of melting in non-summer seasons, and that 76% of melting during foehn conditions occurred when H_S fluxes were large. The combined effect of foehn and warmer air temperatures may explain why the correlation between E_{melt} and H_S is higher in the warmer

seasons of DJF and MAM (Table 2). The negative correlation between E_{melt} and H_L during SON and ANN ($r_{HL,melt}$ = -0.14 and -0.19, respectively, Table 2) suggests that melting in these seasons primarily occurs when air is anomalously warm and dry, driving upward (i.e., negative) H_L fluxes, consistent with foehn conditions. The weak correlation coefficients given in Table 2 between E_{melt} and the turbulent heat fluxes, which are themselves only a proxy for foehn events, cannot conclusively demonstrate the importance of foehn in driving surface melting. However, they add weight to the evidence presented above.

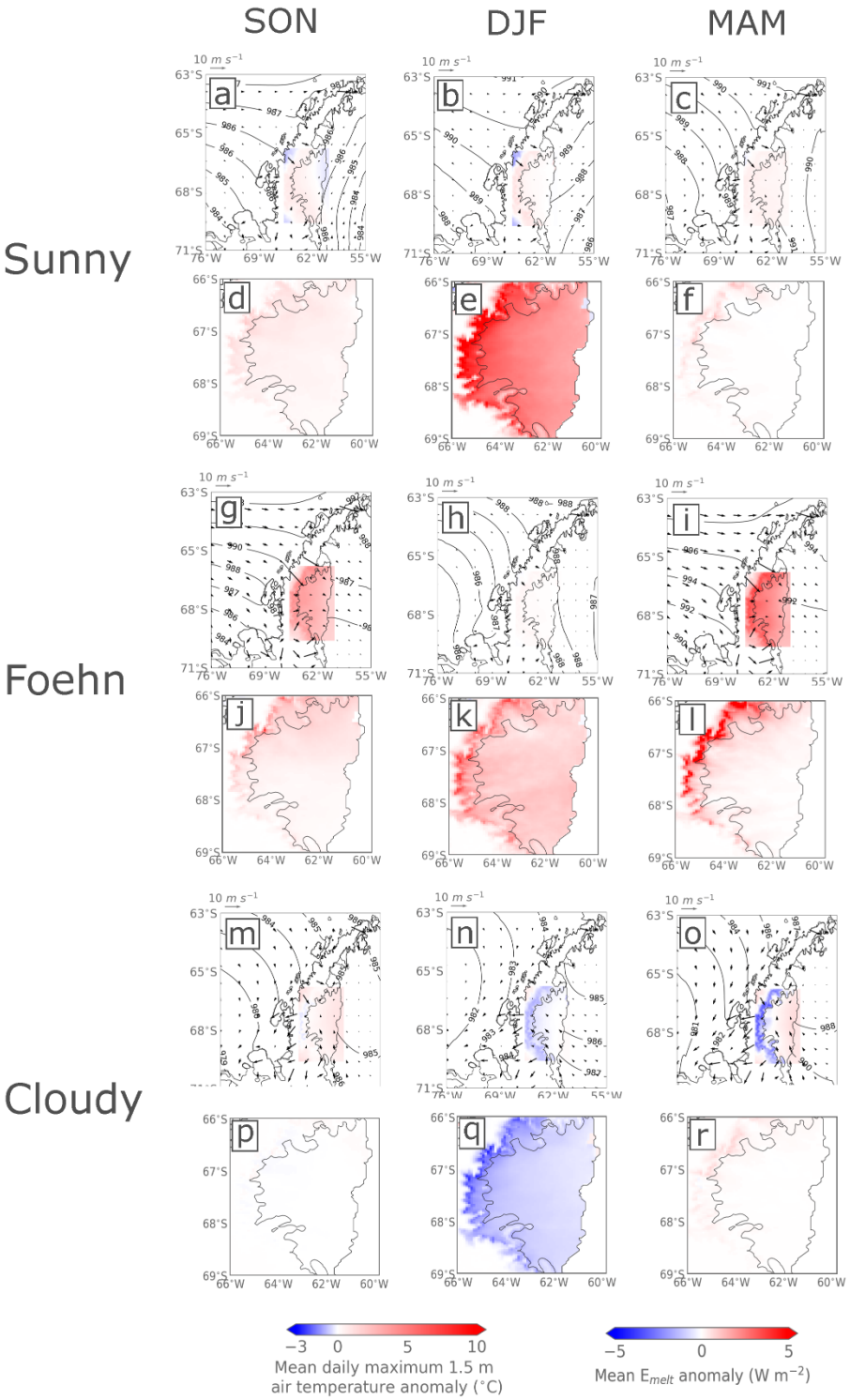
SON
DJF
MAM
Sunny
Foehn
Cloudy
a
b
c
d
e
f
g
h
i
j
k
l
m
n
o
p
q
r
10 m s⁻¹
63°S
65°S
68°S
71°S
66°S
67°S
69°S
76°W
69°W
62°W
55°W
66°W
64°W
60°W
−3 0 5 10
Mean daily maximum 1.5 m air temperature anomaly (°C)
−5 0 5
Mean E_{melt} anomaly (W m^{-2})

Figure 3. As in Figure 2 but showing composited mean synoptic near-surface meteorology (panels a-c, g-i, m-o) and E_{melt} fluxes (panels d-f, j-l, p-r) in 'sunny' (panels a-f), 'foehn' (panels g-l) and 'cloudy' (panels m-r) conditions during SON (left column), DJF (middle column) and MAM (right column) for the hindcast period. JJA is not shown because <0.1% of melting occurs during winter. Contours, vectors, colours and shading are as in Figure 2.

Figure 4 shows mean E_{melt} anomalies in seasons SON, DJF, and MAM for 'sunny foehn', 'non-sunny foehn' and 'sunny non-foehn' conditions, which allows us to further elucidate the relative importance of SW and foehn on melting over Larsen C. In all seasons, 'sunny foehn' conditions account for more positive E_{melt} anomalies than either 'sunny' or 'foehn' conditions alone (e.g., compare Figure 3d-f and 3j-l with Figure 4a-c). In DJF, foehn conditions slightly enhance melting in inlets (Figure 3k), but SW radiation is evidently much more important for driving melt across the ice shelf because when $SW_{\downarrow}$ is low, foehn conditions are associated with negative E_{melt} anomalies across much of Larsen C (Figure 4e). However, in MAM the opposite is true, suggesting that foehn conditions are a more important driver of melt in this season than SW radiation: even when $SW_{\downarrow} > 75^{th}$ percentile, if foehn conditions are not also simulated, E_{melt} anomalies are negative (Figure 4i). In SON, both foehn and sunny conditions must be simulated to generate positive E_{melt} anomalies. E_{melt} anomalies are negative during 'non-sunny foehn' and 'sunny non-foehn' conditions (Figure 4d and 4g), but positive in 'sunny foehn' (Figure 4a), which is consistent with the small positive E_{melt} anomalies associated with both 'foehn' and 'sunny' shown in Figure 3d and 3j.

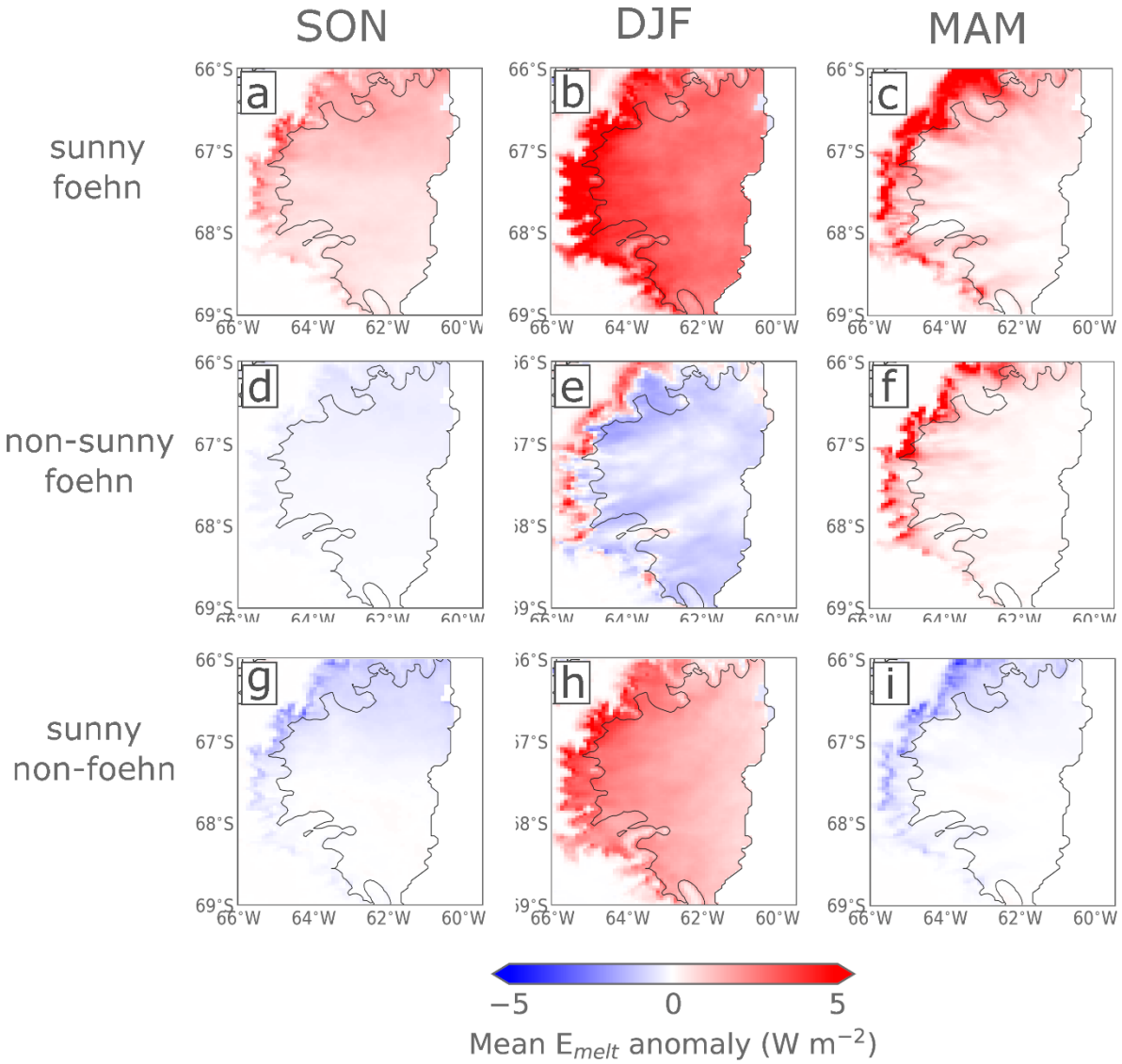

Figure 4. As in Figure 2, but showing seasonal E_{melt} anomalies only for SON (left column), DJF (middle column) and MAM (right column) during three separate conditions for the hindcast period: 'sunny foehn' when $SW_{\downarrow} > 75^{th}$ percentile *and* foehn conditions are simulated (panels a-c); 'non-sunny foehn' when foehn conditions are simulated but $SW_{\downarrow} < 25^{th}$ percentile (panels d-f); and 'sunny non-foehn' when $SW_{\downarrow} > 75^{th}$ percentile is simulated but foehn conditions are not (panels g-i).

3.2.3 Cloud

To examine the role of cloud on surface melting, composites of 'cloudy' conditions are shown in Figure 3m-r. During DJF, cloudy conditions are associated with an easterly flow of maritime air from the Weddell Sea and negative T_{max} anomalies on Larsen C (Figure 3n). This part of the Weddell Sea is typically ice-free during summer, so relatively warm, moist maritime air is advected over the cold ice shelf, resulting in cooling of the air and condensation. Further examination of the hindcast output shows that enhanced $LW_{\downarrow}$ produces positive E_{tot} anomalies and a mean absolute value of 9.3 W m^{-2} over ice shelf areas away from the inlets, but because temperatures typically do not reach the melting point during cloudy periods (mean T_{max} during 'cloudy' conditions is around -1.1°C), and because $SW_{\downarrow}$ is reduced, melt anomalies are negative (Figure 3q). Therefore, despite occurring 62% of the time in DJF, 'cloudy' conditions are associated with just 50% of melt (Table 1). SON composites (Figure 3m and 3p) mirror the DJF composites, with cloudy conditions suppressing melt relative to the climatology. Cloudy conditions occur 62% of the time in SON but are associated with just 57% of melt (Table 1).

During JJA, cloudy conditions, generated by cyclonic flow to the east and southerly winds over Larsen C, are associated with positive T_{max} anomalies (not shown). Table 1 shows that E_{melt} anomalies in JJA are almost zero because melt occurs so infrequently in JJA, but 95% of the melting that does occur is associated with cloudy conditions (91% for high LWP, Table 1). Cloudy composites during MAM (Figure 3o and 3r) are comparable to those during JJA, with cloud enhancing E_{melt}: 69% of MAM melting occurs in cloudy periods, which occur 55% of the time (Table 1).

Cloudy and clear conditions are typified by high and low liquid water path (LWP $> 75^{th}$ percentile and $< 25^{th}$ percentile), respectively, and synoptic conditions and SEB anomalies during 'cloudy' conditions are virtually indistinguishable from those during the 'high LWP' regime (not shown), suggesting the prevalence of liquid-bearing cloud in the hindcast and its importance in determining melt. To avoid repetition, we do not include figures showing high LWP conditions because they are so similar.

The seasonal pattern outlined above is consistent with the correlation coefficients shown in Table 2, which show that E_{melt} is positively correlated with $LW_{\downarrow}$ in MAM, SON and annually ($r_{LW\downarrow,melt} = 0.15$, 0.22 and 0.33, respectively). This supports the notion that $LW_{\downarrow}$ is an important cloud-mediated control on surface melting, as demonstrated by e.g. Zhang et al. (1996) and Gilbert et al. (2020). Cloudy, high LWP conditions may also induce a 'thermal blanketing' effect, whereby $SW_{\downarrow}$ is attenuated and $LW_{\downarrow}$ enhanced so that R_{net} is close to zero or just positive. In these conditions, if H_S and surface temperatures are above zero, melting can result (Ghiz et al., 2021).

Because mean daily T_{max} during cloudy, high LWP conditions is only slightly below the melting point (as noted above) and the large $LW_{\downarrow}$ fluxes associated with cloud produce positive E_{tot} fluxes, this implies that cloud could become

an important driver of surface melt in a warming climate. Surface air temperatures on the eastern Antarctic Peninsula are projected to warm by ~0.5-3°C by 2100 (van Oldenborgh et al., 2013), which would mean the melting point could be reached more frequently in DJF during cloudy periods. This could allow extensive low cloud-mediated melt events to occur such as were observed in Greenland in 2012 (Bennartz et al., 2013) and which have been documented in West Antarctica (Ghiz et al., 2021). As shown in Gilbert et al. (2020), cloud initiates summertime melt by raising surface temperatures and producing an energy surplus (positive E_{tot}), which then persists as cloud glaciation occurs and SW fluxes increase. This can induce a positive feedback if melt occurs in sufficient volume to reduce the surface albedo, because the darker melting surface can then absorb more SW radiation and sustain further melting. Because low-level (liquid) cloud is typically extensive on Larsen C, this melting could occur across the entire ice shelf.

3.2.4 Foehn-induced cloud clearance on Larsen C

The various combinations of 'sunny', 'clear', 'LWP25' and 'foehn' conditions can also be used to examine the importance of cloud clearance on Larsen C, whereby warm, dry foehn air reduces cloud cover and enhances melting by increasing $SW_{\downarrow}$ (Hoinka et al., 1985). While this mechanism has been proposed to explain enhanced melting over the ice shelf, e.g. by Kuipers Munneke et al. (2012); Grosvenor et al. (2014); Cape et al. (2015); King et al. (2017) and Elvidge et al. (2020), its significance has not yet been established across larger spatial and temporal scales on Larsen C.

Foehn clearance can be defined as clear, sunny foehn periods with low LWP, or the coincidence of foehn conditions with any of these criteria. Because model cloud fraction is parameterised according to sub-grid scale variability in moisture, it can be less reliable than prognostic diagnostics like LWP or solar radiation, so the definition is not necessarily as straightforward as the coincidence of clear and foehn periods. Of the times when foehn conditions are detected, 'sunny' conditions also occur 27%, 29% and 31% of the time in MAM, SON and DJF, respectively (Table S2). Because cloudy conditions are so common on Larsen C (occurring 55-62% of the time, as shown in Table 1), 'cloudy foehn' conditions also occur frequently, accounting for 35-59% of foehn periods depending on the season. 'Clear foehn' occur on average approximately five times less frequently (9-13% of foehn periods, Table S2). 'Low LWP foehn', which may include foehn periods where optically thin liquid clouds or high-level ice clouds are present, account for 25-31% of foehn periods and 12-20% of foehn periods are 'high LWP foehn' (Table S2).

Table 3. Co-occurrence of 'sunny', 'cloudy', 'clear', 'high LWP', 'low LWP' and 'foehn' conditions with 'high melt' conditions during each season. The values shown represent the percentage of time during which the conditions overlap with high melt conditions, that is, of the times that high melt conditions are occurring, what percentage of the time the conditions in question also occur.

	DJF	MAM	JJA	SON
Sunny	49.9%	45.5%	0.0%	73.3%
Foehn	23.7%	48.5%	92.3%	40.6%
Cloudy	44.2%	50.8%	84.6%	54.5%
Clear	9.7%	5.3%	0.0%	6.1%
High LWP	9.9%	34.1%	69.2%	40.0%
Low LWP	35.2%	8.3%	0.0%	8.5%
Sunny foehn (sunny + foehn)	12.9%	18.2%	0.0%	27.9%
Clear foehn (clear + foehn)	3.4%	3.0%	0.0%	4.8%
Cloudy foehn (cloudy + foehn)	10.6%	20.5%	76.9%	20.6%
Low LWP foehn (LWP25 + foehn)	9.3%	6.1%	0.0%	3.6%
High LWP foehn (LWP75 + foehn)	2.0%	10.6%	61.5%	12.1%

Table 3 shows how frequently high melt periods coincide with these conditions. Sunny conditions co-occur with 46-73% of high melt periods (excluding JJA when SW radiation is negligible), while foehn and cloudy conditions co-occur with 24-92% and 44-85% of high melt periods, respectively. Clear and high melt conditions co-occur relatively infrequently, coinciding for <10% of the time high melt periods are detected in all seasons, consistent with clear conditions occurring infrequently (7-11% of the time in Table 1). Similarly, in non-summer seasons low LWP periods coincide quite rarely with high melt periods (8% in MAM and 9% in SON, Table 3). In comparison, cloudy/high LWP conditions coincide with a much larger percentage of high melt periods than clear/low LWP conditions (Table 3). In DJF however, while cloudy conditions coincide with a large proportion (44%) of high melt periods, high LWP conditions do not. Instead, low LWP and high melt conditions more commonly co-occur (35%). The importance of cloudy *and* low LWP conditions suggests that optically thin, low-level clouds could be important for driving surface melting over Larsen C during summer, as seen in Greenland and West Antarctica (Bennartz et al., 2013; Ghiz et al., 2021), or that cloud clearance at lower levels could drive melting while high-level ice cloud is present (therefore resulting in a large cloud fraction). The latter would constitute cloud clearance but further investigation is required.

In DJF, when the majority of melting occurs, E_{melt} anomalies averaged across the whole ice shelf are positive during 'sunny foehn', 'low LWP foehn' and 'clear foehn' (1.00, 0.70 and 0.62 W m^{-2}, respectively, Table S2), and near-zero or negative during 'cloudy foehn' and 'high LWP foehn' (0.02 and -0.32 W m^{-2}, respectively, Table S2). In other seasons the largest positive E_{melt} anomalies are associated with cloudy foehn and high LWP foehn (1.02 and 2.03 W m^{-2}, respectively in MAM and 0.31 and 0.54 W m^{-2}, respectively in SON, Table S2).

Periods when all three criteria ('clear foehn', 'low LWP foehn' and 'sunny foehn') all occur together are uncommon, happening during <1% of the hindcast. However, these periods coincide with 1-4% of high melt periods (not shown), imply-

ing that foehn-induced cloud clearance may drive above-average summertime melt when it occurs, but that such conditions occur fairly infrequently. Further examination of the importance of foehn clearance is needed to comprehensively evaluate its role in driving melt.

3.2.5 The influence of large-scale circulation

While the most important first-order processes driving surface melting are SW radiation, foehn and cloud, large-scale circulation variations, associated with patterns like the SAM, ENSO and ASL, exert controls on these processes. For example, the high melt years identified in Part 1 were also SAM+ years, supporting the idea that this atmospheric circulation pattern enhances melting. Table 1 suggests that SAM+ and ENSO- enhance surface melting in DJF and MAM, because the percentage of melt that is associated with them is higher than the percentage of time they occur. Meanwhile SAM-, ENSO+ and ASL conditions suppress melting in all seasons except for ENSO+ in SON (Table 1). This anti-correlation of ENSO/SAM modes (i.e. the co-occurrence of ENSO- and SAM+ conditions and vice versa) is consistent with the findings of e.g. Fogt et al. (2011) noted in section 1. As discussed in section 1, ASL conditions strengthen the flow impinging on the Antarctic Peninsula and so can increase the advection of air over the peninsula mountains (Hosking et al., 2013), therefore enhancing melt over Larsen C.

Figure 5 shows composited mean meteorological conditions and E_{melt} anomalies during SAM+, SAM-, ENSO+, ENSO-, barrier wind and ASL conditions. Anomalies are shown for DJF only, when their absolute influence on E_{melt} is strongest, although they have a larger relative effect on circulation and melting in other seasons. Comparing panels 5d and 5j further confirms that SAM+ and SAM- conditions produce positive and negative E_{melt} anomalies, respectively, especially in the immediate lee of steep terrain. Figure 5c and 5e also show that the circulation patterns in DJF associated with SAM+ and ENSO- are very similar, with weak cyclonic flow west of the Antarctic Peninsula generating weak cross-peninsula flow across Larsen C. This similarity is consistent with the anti-correlation between ENSO and SAM modes previously noted. T_{max} anomalies in Figure 5c and 5e are close to zero, suggesting that SAM+ and ENSO- produce positive melt anomalies (Figure 5d and 5f) via their effect on the SEB, rather than because they raise temperatures. During SAM+ and ENSO- conditions in DJF, the SEB is dominated by $SW_{\downarrow}$, which causes surface melting to be widespread across the ice shelf. The synoptic conditions associated with SAM+ and ENSO- are more extreme during MAM (not shown), when intensive foehn conditions are common (as shown above), and generate positive T_{max}, H_S and E_{melt} anomalies in inlets.

As shown in Table 1 and Figure 5a and 5b, (deep) ASL conditions are associated with positive T_{max} and E_{melt} anomalies over Larsen C during DJF and MAM. However, whereas in DJF the ASL is associated with positive E_{melt} anomalies across the entire shelf (Figure 5b), in MAM (not shown) the anomalies are confined to inlets with a similar pattern to the foehn composite shown in Figure 3l.

Conversely, during SON and JJA ASL conditions are associated with negative T_{max} anomalies and in SON with slightly negative E_{melt} anomalies (not shown). Therefore, despite occurring 36.6% and 11.6% of the time, the ASL is associated with just 19.4% and 0.2% of melting during SON and JJA, respectively (Table 1).

These conditions are non-independent and the similarities between them further suggest that SAM+, ENSO- and (in some seasons) ASL patterns produce flow-over conditions that result in foehn, the importance of which has been demonstrated. The co-occurrence of foehn and SAM+ or ENSO- conditions can also be used to demonstrate the influence of large-scale circulation patterns on mesoscale meteorology. Of the times when foehn conditions are detected, SAM+ conditions also occur 26%, 37%, 23% and 28% of the time for SON, DJF, MAM and JJA, respectively, while ENSO- conditions occur 24%, 32%, 35% and 17% of the time, respectively. This suggests that SAM+ is most important for establishing foehn conditions during DJF while ENSO- is most influential in MAM.

SAM+ has been more robustly linked to foehn occurrence, and its importance is supported by the results presented in Table 4, which shows Pearson correlation coefficients between observed SAM index and modelled foehn wind frequency at inlet and ice shelf stations for all seasons and annually, and Figure 6, which shows the relationship between these variables at inlet stations only. The correlation between annually averaged SAM index and annual mean foehn frequency is 0.52 in inlets and 0.54 at over the ice shelf (both significant at the 95% level, Table 4). This suggests that a more positive SAM index corresponds to periods of higher foehn occurrence, as also shown by e.g. Cape et al. (2015). The largest and most significant Pearson correlation coefficient between seasonal mean SAM index and foehn occurrence (at the 99% level) is found during DJF and weakest (and insignificant) during JJA. Meanwhile, those in SON and MAM are significant at the 95% level (Table 4).

The composites presented in Figure 5 and the correlations between SAM+ and foehn conditions in Table 4 and Figure 6 demonstrate the importance of large-scale atmospheric circulation patterns in establishing mesoscale atmospheric conditions like foehn that promote surface melting on Larsen C.

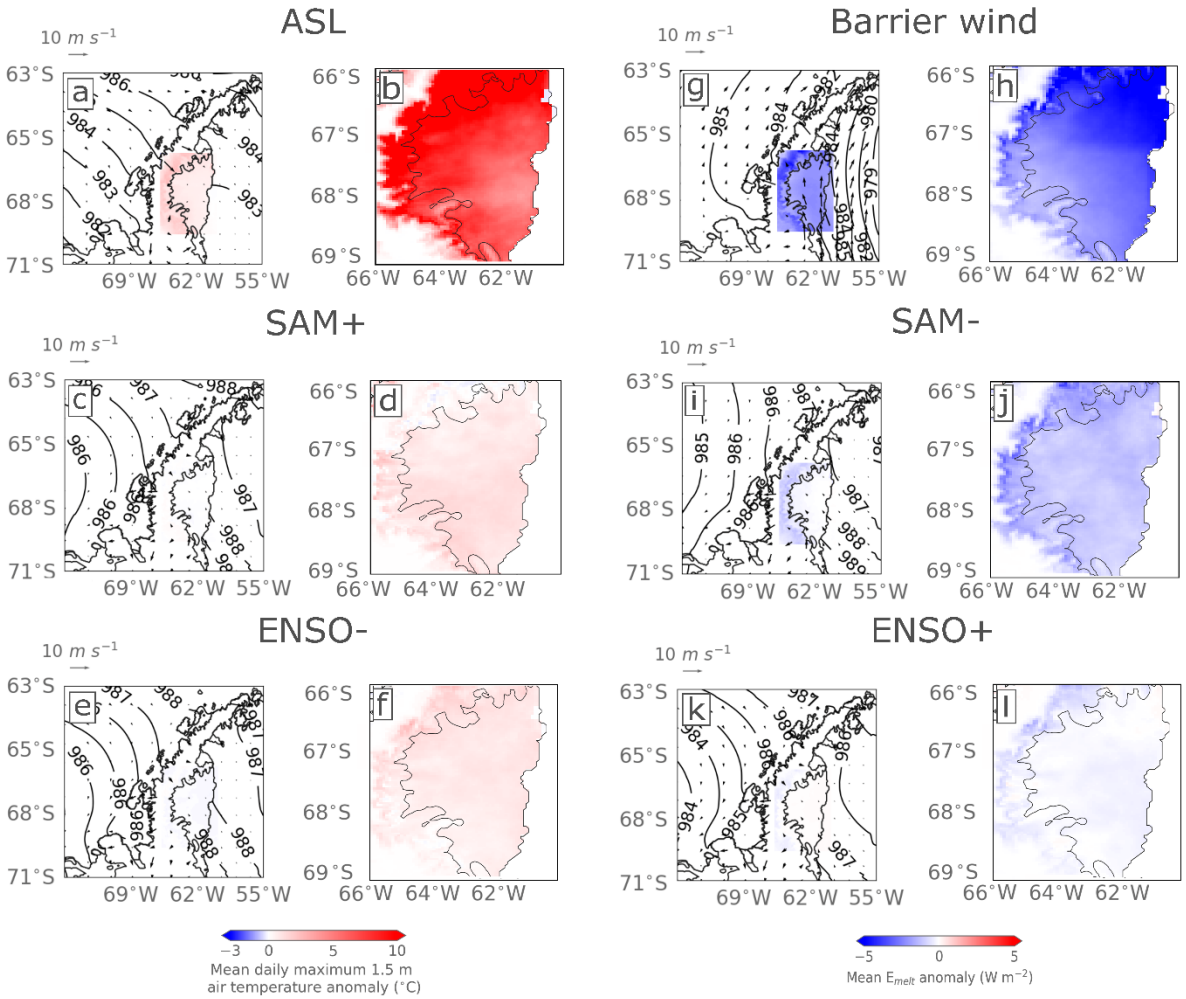

Figure 5. Composited synoptic conditions and mean E_{melt} anomalies for the large-scale circulation patterns examined for the duration of the hindcast: ASL (a, b), SAM+ (c, d), ENSO- (e, f), barrier winds (g, h), SAM- (I, j), and ENSO+ (k, l). Composites are shown for DJF only, when the absolute effect on E_{melt} is largest. Conditions that enhance melt are shown in panels a-f, while conditions that suppress melt are shown in panels g-l. Colours, vectors and contours are as in previous figures.

Table 4. Pearson correlation coefficients between modelled foehn frequency at inlet and ice shelf stations with the observed SAM index for the duration of the hindcast. Correlations that are statistically significant at the 95% level are given in bold, while statistical significance of 99% is indicated with an asterisk.

Season	Inlet	Ice shelf

Season	Inlet	Ice shelf
DJF	**0.66***	**0.62***
MAM	**0.55**	**0.54**
JJA	0.19	0.16
SON	**0.50**	**0.46**
ANN	**0.52**	**0.54**

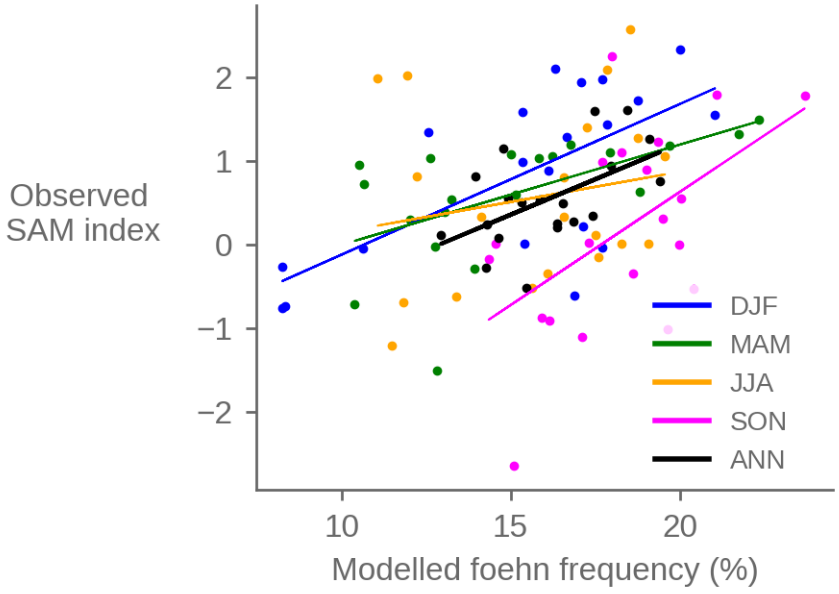

Figure 6. Scatter plot of hindcast modelled seasonal mean foehn occurrence at inlet stations, expressed as a percentage of time, against observed seasonal mean SAM index for the duration of the hindcast, calculated after Marshall (2003). Individual seasons are shown with coloured markers and the regression line for each season is shown in the corresponding colour. The annual mean is indicated with black markers and the solid black line.

3.2.6 Conditions that suppress melt

The focus of this study has been on conditions that enhance surface melting. However, it is evident from Table 1 and Figure 5 that some atmospheric con-

ditions suppress melting, most notably barrier wind, SAM- and ENSO+ conditions. Low melt periods (melt amount $< 25^{\text{th}}$ percentile) are associated in DJF with the development of a southerly barrier jet that delivers cold air from high on the Antarctic plateau, typically established by cyclones in the Weddell Sea that produce coastal easterlies or south-easterlies, resulting in cold T_{max} anomalies over Larsen C (not shown). Barrier wind conditions are associated with extremely negative T_{max} and E_{melt} anomalies across the entire Larsen C ice shelf (Figure 5g and 5h). The temperature anomalies are the primary reason that surface melting is suppressed during these periods, because E_{tot} is affected minimally (anomalies are small). SAM- (Figure 5i and 5j) and ENSO+ conditions (Figure 5k and 5l) also suppress melting relative to DJF climatology because both reduce the flow of air over the peninsula.

For all three types of melt-suppressing conditions, the magnitude of the simulated negative T_{max} anomalies is greater in non-summer seasons, but E_{melt} anomalies are smaller because the majority of melting occurs in DJF. For instance in non-summer seasons, ENSO+ and SAM- conditions are associated with more southerly flow which brings cold continental air over Larsen C, suppressing temperatures and melting. The exception is ENSO- conditions in SON: during these periods small positive T_{max} anomalies are simulated, which drives a very weak positive E_{melt} anomaly.

4 Summary & conclusions

This study has comprehensively evaluated the dominant causes of surface melting on the Larsen C ice shelf in a hindcast simulation of the most recent two decades. Building on previous work that has explored the causes of melt on Larsen C (such as King et al., 2017; Kuipers Munneke et al., 2018; Datta et al, 2019; Wiesenekker et al., 2019; Elvidge et al., 2020 and Gilbert et al., 2020; 2021), this study has systematically ranked the conditions that drive surface melt in order of importance. Many of these conditions overlap and co-occur, and can reinforce or counteract each other. However, the analysis presented here has attempted to isolate the effects of individual drivers of surface melting on Larsen C. The most important drivers can be summarised as follows.

Firstly, SW radiation is the most important driver of melting in DJF, when 90% of melting occurs. Sunny summertime conditions are associated with the highest E_{melt} anomalies of all drivers (Table 1, Figure 3).

Secondly, foehn winds are the most important driver of melt in non-summer seasons, especially MAM, but this only accounts for 10% of annual meltwater production (Table 1, Figure 3). Foehn winds are also important in DJF because they enhance already high melt fluxes, but their influence is secondary to that of $SW_{\downarrow}$ in summer. E_{melt} anomalies are highest in all seasons when sunny and foehn conditions co-occur (Figure 4). Foehn-induced cloud clearance may drive large E_{melt} anomalies but probably occurs relatively infrequently in the hindcast: rather, the occurrence of foehn during already sunny conditions enhances surface melting (Table 3).

Thirdly, clouds - especially those with high LWP - increase $LW_{\downarrow}$ radiation and therefore E_{tot}. However, because temperatures are typically just below the melting point during cloudy conditions, widespread melting does not regularly occur unless temperatures are already unusually high (Figure 3). This suggests that if ongoing atmospheric warming persists, as projected throughout the 21st century, cloud-mediated melting such as is already observed in Greenland and West Antarctica could begin to occur across Larsen C and other ice shelves on the Antarctic Peninsula.

Finally, large-scale circulation influences regional and mesoscale meteorology by establishing dominant flow patterns. Large-scale patterns such as SAM and ENSO and regional features such as the ASL and barrier winds influence atmospheric circulation in the region and can affect the surface meteorology, SEB and melt (Figure 5). Further, large-scale circulation patterns can affect sea ice conditions, which can in turn interact with regional meteorology, for instance moderating the properties of air that flows onto the Larsen C ice shelf.

Modelled foehn frequency is shown to be strongly correlated with an observed SAM index (r = 0.62, Table 4, Figure 6), which suggests that more foehn events, and therefore more melting, could result if the trend towards a more positive SAM that was recorded from the 1960-2000s (Marshall, 2003; Fogt & Marshall, 2020) resumed. While no trends in foehn frequency are evident over the hindcast period, this is likely because we only have 20 years of data and there is considerable interannual variability (c.f. Gilbert et al. 2021).

The trend towards a more positive SAM is expected to resume as greenhouse gas concentrations increase. Rising greenhouse gas concentrations cause the westerly winds associated with SAM+ to strengthen and migrate polewards and will likely outweigh the compensating effects of ozone recovery if emissions continue at current levels (Zheng et al., 2013). Although future changes to ENSO are highly uncertain (Fredriksen et al., 2020), the coupling between ENSO and SAM may also imply a transition towards ENSO- conditions as the positive SAM trend continues. The combination of higher foehn frequency associated with a more positive SAM and rising temperatures related to ongoing global climate change could contribute to greater meltwater production by allowing melt to occur more frequently via the mechanisms outlined above, and for that melt to be more intense. This could lead to the eventual destabilisation of Larsen C via hydrofracturing, with far-reaching implications for global sea level rise. Larsen C has already been identified as an ice shelf at risk of hydrofracturing-induced collapse if warming continues unchecked (Trusel et al., 2015; Gilbert & Kittel, 2021). Quantifying the future fate of the Larsen C ice shelf is beyond the scope of this paper but should be a focus of research to determine change on the Antarctic Peninsula.

Acknowledgments

The authors declare no conflicts of interest. This work was supported by the Natural Environment Research Council through the EnvEast Doctoral Train-

ing Partnership (grant number NE/L002582/1). The authors also acknowledge use of the MONSooN system, a collaborative facility supplied under the Joint Weather and Climate Research Programme, a strategic partnership between the Met Office and the Natural Environment Research Council. The authors gratefully acknowledge Prof. Michiel R. van den Broeke, who kindly provided AWS data.

Hindcast model data can be accessed on the CEDA archive at https://catalogue.ceda.ac.uk/uuid/41c879b06af64 and can be cited as Gilbert, E. (2020): High-resolution regional Met Office Unified Model (UM) climate model hindcast of the Antarctic Peninsula (1998-2017). Centre for Environmental Data Analysis, date of citation. AWS data can be retrieved from https://www.projects.science.uu.nl/iceclimate/aws/.

References

Bell, R. E., Banwell, A. F., Trusel, L. D., & Kingslake, J. (2018). Antarctic surface hydrology and impacts on ice-sheet mass balance. Nature Climate Change, 8(December), 1044–1052. https://doi.org/10.1038/s41558-018-0326-3

Bennartz, R., Shupe, M. D., Turner, D. D., Walden, V. P., Steffen, K., Cox, C. J., Kulie, M. S., Miller, N. B., & Pettersen, C. (2013). July 2012 Greenland melt extent enhanced by low-level liquid clouds. *Nature*, *496*(7443), 83–86. https://doi.org/10.1038/nature12002

Bevan, S. L., Luckman, A. J., Kuipers Munneke, P., Hubbard, B., Kulessa, B., & Ashmore, D. W. (2018). Decline in Surface Melt Duration on Larsen C Ice Shelf Revealed by The Advanced Scatterometer (ASCAT). Earth and Space Science, 5(10), 578–591. https://doi.org/10.1029/2018EA000421

Bozkurt, D., Bromwich, D. H., Carrasco, J., Hines, K. M., Maureira, J. C., & Rondanelli, R. (2020). Recent Near-surface Temperature Trends in the Antarctic Peninsula from Observed, Reanalysis and Regional Climate Model Data. Advances in Atmospheric Sciences, 37, 477–493. https://doi.org/10.1007/s00376-020-9183-x

Cape, M. R., Vernet, M., Skvarca, P., Marinsek, S., Scambos, T., & Domack, E. (2015). Foehn winds link climate-driven warming to ice shelf evolution in Antarctica. Journal of Geophysical Research: Atmospheres, 120(21), 11037–11057. https://doi.org/10.1002/2015JD023465

Center for Climate Prediction (2005). Teleconnection pattern calculation procedures. https://www.cpc.ncep.noaa.gov/products/precip/CWlink/daily_ao_index/history/method.shtml retrieved November 14th 2019.

Clem, K. R., Renwick, J. A., McGregor, J., & Fogt, R. L. (2016). The relative influence of ENSO and SAM on Antarctic Peninsula climate. Journal of Geophysical Research: Atmospheres, 121, 11038–11054. https://doi.org/10.1002/2016JD02495

Datta, R. T., Tedesco, M., Fettweis, X., Agosta, C., Lhermitte, S., Lenaerts, J. T. M., & Wever, N. (2019). The Effect of Foehn-Induced Surface Melt on

Firn Evolution Over the Northeast Antarctic Peninsula. Geophysical Research Letters, 46, 3822–3831. https://doi.org/10.1029/2018GL080845

Dätwyler, C., Grosjean, M., Steiger, N. J., & Neukom, R. (2020). Teleconnections and relationship between ENSO and SAM in reconstructions and models over the past millennium. Climate of the Past, 743–756, 743–756. https://doi.org/10.5194/cp-2019-110

Deb, P., Orr, A., Bromwich, D. H., Nicolas, J. P., Turner, J., & Hosking, J. S. (2018). Summer Drivers of Atmospheric Variability Affecting Ice Shelf Thinning in the Amundsen Sea Embayment, West Antarctica. Geophysical Research Letters, 45(9), 4124–4133. https://doi.org/10.1029/2018GL077092

Dee, D. P., Uppala, S. M., Simmons, A. J., Berrisford, P., Poli, P., Kobayashi, S., … & Bechtold, P. (2011). The ERA-Interim reanalysis: Configuration and performance of the data assimilation system. *Quarterly Journal of the Royal Meteorological Society 137* (656), 553-597. https://doi.org/10.1002/qj.828

Elvidge, A. D., Renfrew, I. A., King, J. C., Orr, A., Lachlan-Cope, T. A., Weeks, M., & Gray, S. L. (2015). Foehn jets over the Larsen C Ice Shelf, Antarctica. Quarterly Journal of the Royal Meteorological Society, 141(688), 698–713. https://doi.org/10.1002/qj.2382

Elvidge, A. D., Renfrew, I. A., King, J. C., Orr, A., & Lachlan-Cope, T. A. (2016). Foehn warming distributions in nonlinear and linear flow regimes: A focus on the Antarctic Peninsula. Quarterly Journal of the Royal Meteorological Society, 142(695), 618–631. https://doi.org/10.1002/qj.2489

Elvidge, A. D., Kuipers Munneke, P., King, J. C., Renfrew, I. A., & Gilbert, E. (2020). Atmospheric drivers of melt on Larsen C Ice Shelf: surface energy budget regimes and the impact of foehn. Journal of Geophysical Research: Atmospheres, 125(17), e2020JD032463. https://doi.org/https://doi.org/10.1029/2020JD032463

Fogt, R. L., Bromwich, D. H., & Hines, K. M. (2011). Understanding the SAM influence on the South Pacific ENSO teleconnection. Climate Dynamics, 36(7), 1555–1576. https://doi.org/10.1007/s00382-010-0905-0

Fogt, R. L., & Marshall, G. J. (2020). The Southern Annular Mode: Variability, trends, and climate impacts across the Southern Hemisphere. *WIREs Climate Change*, *11*(4), e652. https://doi.org/10.1002/wcc.652

Fredriksen, H. B., Berner, J., Subramanian, A. C., & Capotondi, A. (2020). How Does El Niño–Southern Oscillation Change Under Global Warming—A First Look at CMIP6. *Geophysical Research Letters*, *47*(22). https://doi.org/10.1029/2020GL090640

Ghiz, M., Scott, R., Vogelmann, A., Lenaerts, J., Lazzara, M., & Lubin, D. (2021). Energetics of Surface Melt in West Antarctica. *The Cryosphere*, *15*, 3459–3494. https://doi.org/https://doi.org/10.5194/tc-15-3459-2021

Gilbert, E. (2020a). High-resolution regional Met Office Unified Model (UM) climate model hindcast of the Antarctic Peninsula (1998-2017). Centre for Environmental Data Analysis, *16/09/2021* available at: https://catalogue.ceda.ac.uk/uuid/41c879b06af642e9bc8e12d1d0ea3d62

Gilbert, E. (2020b) Atmospheric drivers of surface melting on the Larsen C ice shelf, Antarctic Peninsula. PhD thesis, University of East Anglia.

Gilbert, E., Orr, A., King, J. C., Renfrew, I. A., Lachlan-Cope, T., Field, P. F., & Boutle, I. A. (2020). Summertime cloud phase strongly influences surface melting on the Larsen C ice shelf, Antarctica. Quarterly Journal of the Royal Meteorological Society, 146(729), 1575–1589. https://doi.org/10.1002/qj.3753

Gilbert, E., & Kittel, C. (2021). Surface melt and runoff on Antarctic ice shelves at 1.5°C, 2°C and 4°C of future warming. Geophysical Research Letters, 48, e2020GL091733. https://doi.org/10.1029/2020GL091733

Grosvenor, D. P., King, J. C., Choularton, T. W., & Lachlan-Cope, T. (2014). Downslope foehn winds over the antarctic peninsula and their effect on the larsen ice shelves. Atmospheric Chemistry and Physics, 14(18), 9481–9509. https://doi.org/10.5194/acp-14-9481-2014

Hofer, S., Tedstone, A.J., Fettweis, X. & Bamber, J. (2019) Cloud microphysics and circulation anomalies control differences in future Greenland melt. *Nature Climate Change 9,* 523–528 https://doi.org/10.1038/s41558-019-0507-8

Hoinka, K. P. (1985). What is a Foehn Clearance? *Bulletin of the American Meteorological Society*, *66*(9), 1123–1132. https://doi.org/10.1175/1520-0477(1985)066%3C1123:WIAFC%3E2.0.CO;2

Hosking, J. S., Orr, A., Marshall, G. J., Turner, J., & Phillips, T. (2013). The influence of the amundsen-bellingshausen seas low on the climate of West Antarctica and its representation in coupled climate model simulations. *Journal of Climate*, *26*(17), 6633–6648. https://doi.org/10.1175/JCLI-D-12-00813.1

King, J. C. (1994) Recent climate variability in the vicinity of the Antarctic Peninsula. *International Journal of Climatology*, *14,* 357–369, https://doi.org/10.1002/joc.3370140402

King, J. C., Gadian, A., Kirchgaessner, A., Kuipers Munneke, P., Lachlan-Cope, T. A., Orr, A., Reijmer, C., Van Den Broeke, M. R., Van Wessem, J. M., & Weeks, M. (2015). Validation of the summertime surface energy budget of Larsen C Ice Shelf (Antarctica) as represented in three high-resolution atmospheric models. Journal of Geophysical Research Atmospheres, 120(4), 1335–1347. https://doi.org/10.1002/2014JD022604

King, J. C., Kirchgaessner, A., Orr, A., Luckman, A., Bevan, S., Elvidge, A., Renfrew, I. A., & Kuipers Munneke, P. (2017). The impact of foehn winds on surface energy balance and melt over Larsen C Ice Shelf, Antarctica. Journal of Geophysical Research: Atmospheres, 122(22), 12062–12076. https://doi.org/10.1002/2017JD026809

Kuipers Munneke, P., Van Den Broeke, M. R., King, J. C., Gray, T., & Reijmer, C. H. (2012). Near-surface climate and surface energy budget of Larsen C ice shelf, Antarctic Peninsula. Cryosphere, 6(2), 353–363. https://doi.org/10.5194/tc-6-353-2012

Kuipers Munneke, P., Luckman, A. J., Bevan, S. L., Gilbert, E., Smeets, C. J. P. P., Van Den Broeke, M. R., Wang, W., Zender, C., Hubbard, B., Ashmore, D., Orr, A., & King, J. C. (2018). Intense winter surface melt on an Antarctic ice shelf. Geophysical Research Letters, 45, 7615–7623. https://doi.org/10.1029/2018GL077899

Laffin, M. K., Zender, C. S., Singh, S., Van Wessem, J. M., Smeets, C. J. P. P., & Reijmer, C. H. (2021). Climatology and Evolution of the Antarctic Peninsula Föhn Wind-Induced Melt Regime From 1979–2018. *Journal of Geophysical Research: Atmospheres*, *126*(4), 1–19. https://doi.org/10.1029/2020JD033682

Liu, H., Jezek, K. C., Li, B., & Zhao, Z. (2015). RadarSat Antarctic Mapping Project Digital Elevation Model, version 2. NSIDC; NASA National Snow and Ice Data Center Distributed Active Archive Center. https://doi.org/https://doi.org/10.5067/8JKNEW6BFRVD

Marshall, G. J. (2003). Trends in the Southern Annular Mode from observations and reanalyses. Journal of Climate, 16(24), 4134–4143. https://doi.org/10.1175/1520-0442(2003)016%3c4134:TITSAM%3e2.0.CO;2

Marshall, G. J., Orr, A., van é, N. P. M., & King, J. C. (2006). The impact of a changing Southern Hemisphere Annular Mode on Antarctic Peninsula summer temperatures. Journal of Climate, 19(20), 5388–5404. https://doi.org/10.1175/JCLI3844.1

Orr, A., D. Cresswell, G. J. Marshall, J. C. R. Hunt, J. Sommeria, and C. G. Wang (2004), A 'low-level' explanation for the recent large warming trend over the western Antarctic Peninsula involving blocked winds and changes in zonal circulation, *Geophysical. Research Letters* 31, L06204, https://doi.org/10.1029/2003GL019160.

Orr, A., Marshall, G. J., Hunt, J. C. R., Sommeria, J., Wang, C.-G., van Lipzig, N. P. M., Cresswell, D., & King, J. C. (2008). Characteristics of Summer Airflow over the Antarctic Peninsula in Response to Recent Strengthening of Westerly Circumpolar Winds. Journal of the Atmospheric Sciences 65 (4), 1396–1413. https://doi.org/10.1175/2007JAS2498.1

Orr, A., A. Kirchgaessner, J. King, T. Phillips, E. Gilbert, A. Elvidge, M. Weeks, A. Gadian, P. Kuipers Munneke, M. van den Broeke, S. Webster, and D. McGrath (2021), Comparison of kilometre and sub-kilometre scale simulations of a foehn wind event over the Larsen C Ice Shelf using the Met Office Unified Model (MetUM), Quarterly Journal of the Royal Meteorological Society, https://doi.org/10.1002/qj.4138.

Parish, T. R. (1983) The influence of the Antarctic Peninsula on the wind field

over the western Weddell Sea. *Journal of Geophysical Research*, **88**, 2684–2692, https://doi.org/10.1029/JC088iC04p02684

Reynolds, R. W., Smith, T. M., Liu, C., Chelton, D. B., Casey, K. S., & Schlax, M. G. (2007). Daily high-resolution-blended analyses for sea surface temperature. Journal of Climate, 20 (22), 5473–5496. https://doi.org/10.1175/2007JCLI1824.1

Scambos, T. A., Hulbe, C., Fahnestock, M. & Bohlander, J. (2000). The link between climate warming and break-up of ice shelves in the Antarctica Peninsula. Journal of Glaciology, 46(154), 516–530. https://doi.org/10.3189/172756500781833043

Scambos, T., Hulbe, C., & Fahnestock, M. (2003). Climate-induced ice shelf disintegration in the Antarctic Peninsula. In E. Domack, A. Levente, A. Burnet, R. Bindschadler, P. Convey, & M. Kirby (Eds.), Antarctic Peninsula Climate Variability: Historical and Paleoenvironmental Perspectives (Vol. 79, pp. 79–92). https://doi.org/doi:10.1029/AR079p0079

Schwerdtfeger, W., (1975). The effect of the Antarctic Peninsula on the temperature regime of the Weddell Sea. *Monthly Weather Review 103*, 45–51, https://doi.org/10.1175/1520-0493(1975)103%3c0045:TEOTAP%3e2.0.CO;2

Takane, Y., & Kusaka, H. (2011). Formation mechanisms of the extreme high surface air temperature of 40.9°C observed in the Tokyo metropolitan area: Considerations of dynamic foehn and foehnlike wind. *Journal of Applied Meteorology and Climatology*, *50*(9), 1827–1841. https://doi.org/10.1175/JAMC-D-10-05032.1

Trusel, L. D., Frey, K. E., Das, S. B., Karnauskas, K. B., Kuipers Munneke, P., van Meijgaard, E., & van den Broeke, M. R. (2015). Divergent trajectories of Antarctic surface melt under two twenty-first-century climate scenarios. Nature Geoscience, 8(12), 927–932. https://doi.org/10.1038/ngeo2563

Turner, J., Phillips, T., Hosking, J. S., Marshall, G. J., & Orr, A. (2013). The Amundsen sea low. International Journal of Climatology, 33(7), 1818–1829. https://doi.org/10.1002/joc.3558

Turton, J. V., Kirchgaessner, A., Ross, A. N., & King, J. C. (2018). The spatial distribution and temporal variability of föhn winds over the Larsen C ice shelf, Antarctica. Quarterly Journal of the Royal Meteorological Society, 144(713), 1169–1178. https://doi.org/10.1002/qj.3284

Turton, J. V., Kirchgaessner, A., Ross, A., King, J., & Kuipers Munneke, P. (2020). The influence of föhn winds on annual and seasonal surface melt on the Larsen C Ice Shelf, Antarctica. *The Cryosphere Discussions*, *14*, 4165–4180. https://doi.org/10.5194/tc-2020-72

van Lipzig, N. P. M., Marshall, G. J., Orr, A., & King, J. C. (2008). The relationship between the Southern Hemisphere annular mode and Antarctic Peninsula

summer temperatures: Analysis of a high-resolution model climatology. Journal of Climate 21 (8), 1649–1668. https://doi.org/10.1175/2007JCLI1695.1

Van Wessem, J. M., Reijmer, C. H., Van De Berg, W. J., Van Den Broeke, M. R., Cook, A. J., Van Ulft, L. H., & Van Meijgaard, E. (2015). Temperature and wind climate of the Antarctic Peninsula as simulated by a high-resolution Regional Atmospheric Climate Model. Journal of Climate, 28(18), 7306–7326. https://doi.org/10.1175/JCLI-D-15-0060.1

Wiesenekker, J. M., Munneke, P. K., van den Broeke, M. R., & Paul Smeets, C. J. P. (2018). A multidecadal analysis of Föhn winds over Larsen C ice shelf from a combination of observations and modeling. Atmosphere, 9(5). https://doi.org/10.3390/atmos9050172

Zhang, T., Stamnes, K., & Bowling, S. A. (1996). Impact of Clouds on Surface Radiative Fluxes and Snowmelt in the Arctic and Subarctic. *Journal of Climate*, *9*(9), 2110–2123. https://doi.org/10.1175/1520-0442(1996)009%3c2110:IOCOSR%3e2.0.CO;2

Zheng, F., Li, J., Clark, R. T., & Nnamchi, H. C. (2013). Simulation and projection of the Southern Hemisphere annular mode in CMIP5 models. *Journal of Climate*, *26*(24), 9860–9879. https://doi.org/10.1175/JCLI-D-13-00204.1